Communication Papers of the 21st Conference on Computer Science and Intelligence Systems (FedCSIS) pp. 81–88
DOI: 10.15439/2026F8443
ISSN 2300-5963 ACSIS, Vol. 49

Cosine Colorization for Enhancement of Magnetic Resonance Angiography (MRA)

Modupe Odusami
0000-0003-1082-185X
Department of Applied Informatics
Vytautas Magnus University, Akademija
Lithuania
modupe.olufunke.odusami@vdu.lt

Robertas Damaševičius
0000-0001-9990-1084
Department of Applied Informatics
Vytautas Magnus University, Akademija
Lithuania
robertas.damasevicius@vdu.lt

Olusola Abayomi-Alli
0000-0003-2513-5318
Faculty of Fundamental Sciences
Vilnius Gediminas Technical University
Vilnius, Lithuania
olusola-oluwakemi.abayomi-alli@vilniustech.lt

Rytis Maskeliūnas
0000-0002-2809-2213
Centre of Real Time Computer Systems
Kaunas University of Technology
Kaunas, Lithuania
rytis.maskeliunas@ktu.lt

***Abstract*—Non-invasive imaging modalities play a crucial role in healthcare. Magnetic resonance angiography (MRA) has enhanced access to blood vessel information. MRA grayscale preserves anatomical fidelity but offers limited perceptual separation. This study investigates the use of cosine colorization to enhance feature discrimination in MRA. Cosine colorization utilizes the Frangi vesselness filter combined with statistical thresholding to isolate vascular regions. Quantitative and statistical evaluations were conducted on 20 MRA volumes, comparing grayscale baselines with full-volume and vessel-restricted cosine mappings. While full-volume colorization introduces structural distortion (SSIM ≈ 0.85 and NMSE ≈ 0.018), the vessel-restricted approach maintains near-perfect anatomical fidelity (SSIM ≈ 1.0 and NMSE ≈ 0). Statistical analysis confirms significant improvements in perceptual separability ($p < 10^{-5}$) without degradation of structural metrics for the vessel-restricted cosine approach. The results show that this approach provides an interpretable enhancement of vascular structures.**

***Index Terms*—Cosine Colorization, Enhancement, Magnetic Resonance Angiography, Vessel-Restricted Mapping.**

I. Introduction

THE Magnetic Resonance Angiography (MRA) imaging modality provides information on blood vessels without exposing patients to ionizing radiation [1]. MRA volumes are typically visualized using grayscale colormaps in clinical practice [2]. The application of windowing techniques in which image values are connected to corresponding shades of gray levels has been used to improve the intensity range of images [2]. The complexity of distinguishing MRA vessels from adjacent structures often poses high contrast resolution and limited perceptual clarity of MRA representations [3]. Colorization has long been understood as an effective way to enhance visual perception, as it enriches image representation by introducing chromatic information that adds a perceptual dimension [3]. The ability to colorize grayscale images can greatly improve their visual quality and make them easier to interpret [4]. In medical imaging, however, colorization must be carefully designed to preserve anatomical structure and avoid introducing misleading artifacts [5], [6]. Nonlinear color-mapping approaches have been shown to improve visual distinction. By enhancing structural features, they often make anatomical information more noticeable than in standard grayscale images [7], [8]. However, their effectiveness in preserving anatomical integrity—particularly in volumetric angiographic data—has not yet been thoroughly investigated.

The use of colorization techniques in medical imaging shows that volume visualization capabilities could be improved, and a well-interpretable rendering of complex data could be achieved [9]. In multi-modal PET and CT imaging, dual-threshold colorization allows for better observation and a clear distinction between varying levels of metabolic activity. Similarly, the application of colorization to 3D MRI volumes facilitates the generation of photorealistic 3D renderings, bypassing the limitations of manual transfer functions while maintaining structural integrity [10]. Furthermore, in 3D spectral OCT of the retina, adaptive color mapping enhances instrument visibility and contrast, while visually setting apart semantic regions to inform clinicians of data reliability [10].

We focus specifically on cosine-based colorization as a minimal and interpretable transformation for MRA visualization. Given a normalized grayscale intensity field, we consider a cosine mapping [11] and a mixed cosine–grayscale formulation [12] that preserves luminance structure while introducing controlled chromatic variation. This study aims to characterize trade-offs inherent in periodic color mappings, thereby providing a foundation for subsequent work on constrained optimization and more flexible colorization models.

The main contributions of this work are as follows:

©2026, PTI

- Systematic evaluation of cosine-based colorization for MRA visualization.
- Analysis of the impact of full-volume versus vessel-restricted cosine mappings on anatomical fidelity and perceptual discriminability.
- Introduction of a quantitative evaluation framework combining structural and perceptual metrics for assessing medical image colorization.

II. Literature Review

MRA volumes are conventionally visualized using grayscale colormaps, where voxel intensities are mapped directly to gray levels for display. In clinical practice, grayscale visualization remains the default mode for examining vascular morphology and structural continuity [13]. To improve visibility within grayscale displays, a windowing technique was utilized for maximum intensity projections to adjust the visual representation of the arterial segments for the diagnosis of acute ischemic stroke [14]. Furthermore, windowing was used to ensure that the representation of intra-aneurysmal flow was clear enough to be separated from surrounding structures for quantitative measurement [15]. However, windowing operates strictly through linear or piecewise-linear remapping of intensity values and does not introduce additional perceptual dimensions beyond luminance contrast.

Colorization techniques in medical imaging enhanced visual interpretation. Colorization with semantic segmentation, where region identity constrains color assignment and helps preserve structural boundaries. However, these methods rely on accurate segmentation and typically require annotated data. Another approach leverages domain-specific priors, such as region-of-interest (ROI) masks or anatomical constraints, to localize colorization. This can reduce global distortion and preserve contextual information, although it does not inherently guarantee consistency in luminance or intensity ordering within the colored regions.

Nonlinear extensions, such as gamma or logarithmic mappings, have been used to highlight particular intensity in selected regions [16], [17]. However, these approaches operate through monotonic remapping and only provide intensity scaling [18]. Hue-based ramps introduce chromatic variation and can improve perceptual separation. Nevertheless, they are usually designed for general-purpose visualization [19]. Periodic mappings, on the other hand, provide controlled and reproducible chromatic variation throughout the intensity domain by defining color as an oscillatory function of intensity. By parameterizing color channels using periodic functions like sine or cosine, these mappings allow for exact control over frequency and phase, providing a simplified and comprehensible way to modify color patterns [20]. However, the effect of cosine-based color mappings in medical imaging, particularly with respect to anatomical fidelity, luminance consistency, and intensity ordering, has not been comprehensively evaluated.

Since there is no ground-truth color reference, the assessment of colorization in medical imaging is based on how well the converted image preserves structural and functional information from its original grayscale data. Among the most important factors to take into account are maintaining brightness consistency, intensity ordering, and visual aberrations, including distortions.

III. Methods

The pipeline used in this study is illustrated in Fig. 1. The pipeline includes dataset preparation and normalization of the input 3D MRA volume, production of representation variations, vessel-restricted masking for localized colorization, and quantitative evaluation. First, the input MRA volume is normalized and represented as a grayscale baseline. Then, cosine colorization is applied in two ways: as a full-volume mapping and as a vessel-restricted mapping. For the vessel-restricted representation, a vessel mask is obtained using multiscale Frangi vesselness filtering, anatomical foreground and central masking, and statistical thresholding. Finally, the resulting representations are compared using structural, ordering, and perceptual evaluation metrics.

A. Dataset

The dataset used in this study is the Magnetic Resonance Angiography Atlas Dataset from https://www.nitrc.org/projects/icbmmra/, consisting of sixty-one images of healthy volunteers. This study used 20 three-dimensional MRA healthy volumes for the experiment. The study is concerned with the evaluation of cosine-based colorization; the subset was selected for a controlled paired comparison of the grayscale, full-volumetric, and vessel-restricted representations.

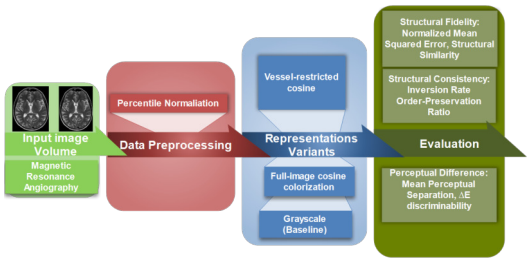

Fig. 1. The evaluation pipeline

B. Data Representation

Let $V(x, y, z) \in [0, 1]$ denote a normalized 3D MRA volume.

A percentile–based min–max scaling normalization technique was applied on the input image volume [21].

To enable direct comparison with colorized outputs, the grayscale volume is replicated across three channels as shown in Eq. (1)

$$\mathrm{GrayB}(x) = [V(x), V(x), V(x)] \tag{1}$$

C. Vessel-Restricted Application

To avoid unwanted color patterns in non-vascular tissue [22], cosine colorization is applied only within vessel regions using a vesselness-based region-of-interest (ROI) mask derived from multiscale filtering and statistical thresholding.

1) Multiscale Frangi Vesselness: Following the Hessian-based formulation described in [23]. The Gaussian filter G(x,s) is applied to the normalized image through convolution to suppress high-frequency noise. For each scale $s \in \{1.0, 2.0, 3.0, \dots\}$, the scale-space representation is:

$$V_s(x) = V_{01}(x) * G(x, s), \tag{2}$$

where $G(x, s)$ is a Gaussian kernel with standard deviation s.

The Frangi parameters are fixed to: $\beta = 0.5, \quad \gamma = 12$.

Multiscale responses are averaged (mean) to improve robustness [24], as computed in Eq. (3).

$$S(x) = \frac{1}{N_s} \sum_s V_f(x, s) \tag{3}$$

where $V_f(x, s)$ is the Frangi vesselness response at scale s, and N is the number of scales.

2) Anatomical Foreground and Central Masking: To reduce artifacts near the cortical rim and avoid false positives caused by image boundaries, vessel extraction is limited to the inner anatomical region [25]. A foreground mask M_{fg} is computed from $V(x)$ using Otsu thresholding [25]. A 3D Euclidean distance transform is then computed inside M_{fg}, and a central mask is defined as

$$M_{\text{central}} = \{x \mid \text{dist}(x, \partial M_{fg}) > d\}, \tag{4}$$

where $d = 20$ voxels.

3) Statistical Vessel Extraction: Vessel regions are defined using a statistical criterion computed within the central mask [26]. The vessel threshold is defined as

$$\tau = \mu_c + k\sigma_c, \tag{5}$$

where μ_c and σ_c are the mean and standard deviation of S_c, and $k = 0.4$. The vessel mask is then defined as

$$M_{\text{vessel}} = \{x \mid S(x) > \tau\}. \tag{6}$$

D. Cosine Color Mapping

The cosine function is used to form smooth and continuous variations in color based on the input intensity values [11]. Cosine colorization embeds grayscale intensities into RGB channels using periodic cosine functions in Eq. (7).

$$\begin{aligned} R &= \frac{1 + \cos(2\pi f I)}{2} \\ G &= \frac{1 + \cos(2\pi f I + 0.5\phi)}{2} \\ B &= \frac{1 + \cos(2\pi f I + \phi)}{2} \end{aligned} \tag{7}$$

where f controls frequency and ϕ controls phase offset. The parameters were fixed to $f = \pi/3$ and $\phi = 2\pi/3$ to provide a slow smooth color modulation with separate RGB phase responses. These values were used as a controlled base line, not an optimized setting.

E. Vessel-Only Cosine Application

Cosine mapping is applied only where $x \in M_{\text{vessel}}$ shown.

$$V_{\text{RGB}}(x) = \begin{cases} (R(x), G(x), B(x)), & x \in M_{\text{vessel}} \\ (0, 0, 0), & \text{otherwise} \end{cases} \tag{8}$$

This isolates colorization to vascular structures and prevents visual distortion in surrounding tissue.

F. Mixed Cosine–Grayscale Representation

To preserve luminance structure while introducing chromatic variation, a mixed representation is defined:

$$V_{\text{mix}}(x) = (1 - \alpha)\,\text{GrayB}(x) + \alpha\, V_{\text{RGB}}(x) \tag{9}$$

where $\alpha \in [0, 1]$ controls the contribution of colorization.

Each experiment's blending coefficient was set to $\alpha = 0.10$ to enable a subtle chromatic enhancement.

G. Evaluation Metrics

Metrics were chosen to evaluate anatomical fidelity, intensity-order preservation, and vessel-background separability. Normalized Mean Squared Error (NMSE) and Structural Similarity (SSIM) measure luminance consistency with the original grayscale MRA; order-preservation ratio (OPR) and inversion rate assess preservation of vessel intensity ordering; and CIELAB-based ΔE, $\Delta Ed'$, and local contrast measure perceptual vessel distinction.

1) Structural fidelity: Structural fidelity was evaluated to determine how well the colorization process preserves the original grayscale appearance of the MRA volume. Since colorization modifies the RGB channels while the anatomical information is encoded primarily in image luminance, the colorized representation was first converted to a luminance image and then compared with the original normalized grayscale volume. Let $V(x)$ denote the normalized grayscale volume and let $T(x) = [R, G, B]$ denote the corresponding colorized output. The luminance of the colorized image was computed using the standard sRGB/Rec. 709 weighting coefficients [27]:

$$Y_T(x) = 0.2126\, R(x) + 0.7152\, G(x) + 0.0722\, B(x). \tag{10}$$

Similarity between luminance image and original grayscale volume was first quantified using the Normalized Mean Squared Error (NMSE), which measures the average reconstruction error relative to the energy of the reference image:

$$\mathbf{NMSE} = \frac{\text{mean}\big((Y_T - V)^2\big)}{\text{mean}\big(V^2\big) + 10^{-8}}. \tag{11}$$

Lower NMSE values indicate better preservation of the original luminance structure, with a value of zero corresponding to perfect agreement.

To complement this pixel-wise error measure, the Structural Similarity Index (SSIM) was computed to evaluate the preservation of local structural information, including luminance, contrast, and spatial organization:

$$\mathbf{SSIM} = \text{SSIM}(Y_T, V). \tag{12}$$

Unlike NMSE, which measures absolute reconstruction error, SSIM emphasizes perceptually meaningful structural consistency between the original grayscale image and the luminance of the colorized representation. An SSIM value approaching one indicates that the colorization preserves the anatomical structure with minimal perceptual distortion.

2) Order preservation: To evaluate whether the proposed colorization preserves the relative ordering of vessel intensities, an order-preservation analysis was performed within the vessel region Ω_v. Rather than comparing absolute intensity values, this analysis examines whether the sign of the intensity difference between neighboring vessel voxels remains unchanged after colorization. Preserving this ordering is important because local intensity relationships contribute to the visual interpretation of vessel continuity and branching.

For each pair of adjacent vessel voxels (x_i, x_{i+1}), the direction of the intensity difference in the original grayscale image and the luminance component of the colorized image was computed as

$$\begin{aligned} d_{\text{ref}}(i) &= \operatorname{sign}\big(V(x_i) - V(x_{i+1})\big), \\ d_{\text{test}}(i) &= \operatorname{sign}\big(Y_T(x_i) - Y_T(x_{i+1})\big), \end{aligned} \tag{13}$$

where $V(x)$ denotes the normalized grayscale intensity and $Y_T(x)$ represents the luminance of the colorized representation. Only voxel pairs with non-zero reference differences were considered, i.e., $d_{\text{ref}}(i) \neq 0$, to avoid ambiguous comparisons between equal-intensity voxels.

Order Preservation Ratio (OPR) measures the ratio of voxel pairs whose ordering is maintained after colorization:

$$\mathbf{OPR} = \frac{1}{|I|} \sum_{i \in I} \mathbf{1}\big[d_{\text{ref}}(i) = d_{\text{test}}(i)\big]. \tag{14}$$

A value of $\mathbf{OPR} = 1$ indicates perfect preservation of local intensity ordering, whereas smaller values indicate increasing disruption of the original ordering.

To quantify the extent of ordering errors, the inversion rate was also computed as the proportion of voxel pairs whose relative ordering is completely reversed:

$$\mathbf{Inversion} = \frac{1}{|I|} \sum_{i \in I} \mathbf{1}\big[d_{\text{ref}}(i) = -d_{\text{test}}(i)\big]. \tag{15}$$

A low inversion rate indicates that the colorization introduces few ordering reversals, thereby preserving the local intensity relationships that characterize vascular anatomy.

3) Perceptual separability: was evaluated to quantify how clearly the colorized vessel regions can be distinguished from their immediate local background. For this purpose, the RGB representation T was first converted into the perceptually motivated CIELAB color space: $(L, a, b) = \text{Lab}(T)$. Let Ω_v denote the vessel region and let Ω_r denote the surrounding ring region used as the local background. The mean CIELAB values of the ring region were used as the local background reference. For each vessel voxel $x \in \Omega_v$, perceptual difference from surrounding background was computed as

$$\Delta E(x) = \sqrt{\big(L - \mu_r(L)\big)^2 + \big(a - \mu_r(a)\big)^2 + \big(b - \mu_r(b)\big)^2}. \tag{16}$$

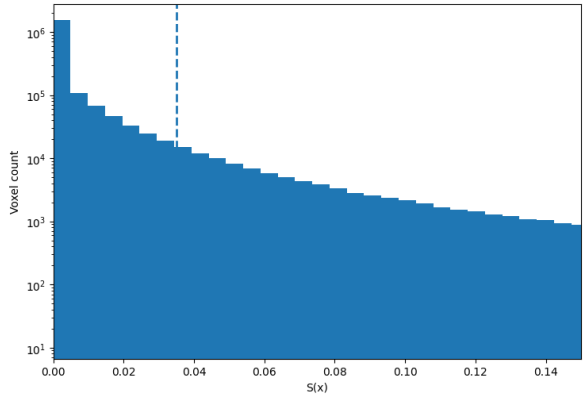

Fig. 2. Frangi vesselness $S(x)$ distribution inside the central mask.

Average vessel-to-background perceptual separation was obtained by averaging $\Delta E(x)$ over all voxels in the vessel region:

$$\Delta E_{\text{mean}} = \frac{1}{|\Omega_v|} \sum_{x \in \Omega_v} \Delta E(x). \tag{17}$$

Discriminability was quantified using a d'-style measure. This metric compares the separation between the vessel and ring distributions relative to their pooled variability:

$$\Delta E\, d' = \frac{|\mu_v - \mu_r|}{\sqrt{0.5(\sigma_v^2 + \sigma_r^2)} + 10^{-8}}. \tag{18}$$

Here, μ_v and σ_v denote the mean and standard deviation of the vessel-region perceptual values, while μ_r and σ_r denote the corresponding statistics for the local ring background. A larger ΔE_{mean} or $\Delta E\, d'$ indicates stronger perceptual separation between vessels and adjacent tissue.

H. Statistical Analysis

A two-sided paired t-test was utilized to assess changes in mean values under the assumption of approximate normality, and the Wilcoxon signed-rank test was used as a non-parametric alternative. Statistical significance was computed at $p < 0.05$.

IV. Result

A. Validation of Vessel Mask

The statistical threshold $\tau = \mu_c + 0.4\sigma_c$ successfully separates low-response background voxels from high-confidence vessel regions, as illustrated in Fig. 2. The dashed vertical line indicates the statistical threshold $\tau = \mu_c + 0.4\sigma_c$.

Fig. 3 shows an overlay of vesselness values M_{central} and the extracted vessel mask M_{vessel}, where the distribution of vesselness values for the extracted mask M_{vessel} is clearly shifted toward higher responses compared to the central mask.

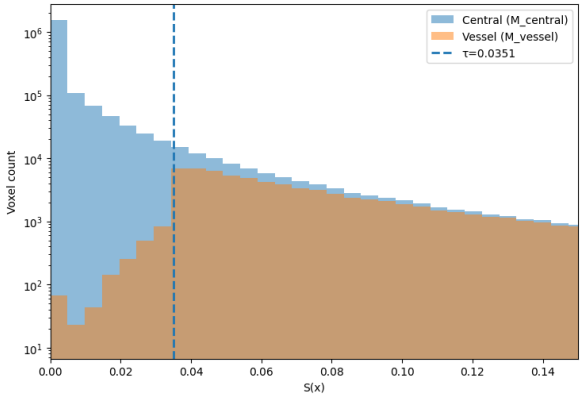

Fig. 3. Central vs. vessel distributions of $S(x)$.

B. Single-Image Quantitative Analysis

The grayscale (baseline), full-volume cosine mapping, and vessel-restricted cosine mapping were evaluated. Table 1 summarizes the quantitative metrics for a single image analysis.

The grayscale image shows NMSE $= 0.000000$, SSIM $= 1.000000$, OPR $= 0.998405$, and zero inversion. It also gives baseline perceptual separability, with $L_{d'} = 0.749028$, chromatic discriminability $= 0.732236$, and $\Delta E_{d'} = 0.224801$.

A quantifiable structural distortion, with NMSE $= 0.018082$ and SSIM $= 0.847326$, is produced with the use of full-volume cosine mapping. Although global intensity ordering stays mostly preserved (OPR $= 0.997503$), a non-negligible level of inversion rate 0.015662 is introduced. Regarding perceptual characteristics, full cosine mapping lowers chromatic discriminability (Chroma $d' = 0.601273$) and overall perceptual separation ($\Delta E_{\text{mean}} = 8.909666$), while only marginally increasing $\Delta E_{d'} = 0.236465$. Vessel-restricted cosine mapping preserves anatomical structure with near-perfect fidelity (NMSE $= 0.000001$, SSIM $= 0.999993$), matching the grayscale baseline in both OPR (0.998405) and inversion (0.000000). Vessel-restricted mapping improves chromatic discriminability (Chroma $d' = 0.795021$) relative to both grayscale and full mapping, while maintaining comparable luminance discriminability ($L_{d'} = 0.748340$) and local contrast (0.083362). It slightly increases perceptual separation ($\Delta E_{\text{mean}} = 10.190250$) and achieves $\Delta E_{d'} = 0.232772$a comparable result to full mapping but without associated distortions.

C. Twenty-Images Quantitative Analysis

To assess consistency, the pipeline was applied to all 20 MRA volumes, and the same metrics were used to assess the grayscale, full-volume cosine, and vessel-restricted cosine mappings. Table 2. Fig. 5, Fig. 6, Fig. 7, Fig. 8, Fig. 9, and Fig. 10 show that the trends observed in the single-image analysis were consistent across the 20-volume subset. The ring is the local background around vessels, used to evaluate how well vessels stand out from nearby tissue.

D. Statistical Analysis of Quantitative Metrics

For vessel versus grayscale, the difference was highly significant (t-test $p < 10^{-6}$, Wilcoxon $p = 2\times10^{-6}$). Similarly, vessel versus full-image cosine mapping showed significant improvement (t-test $p = 10^{-6}$, Wilcoxon $p = 2.7\times10^{-5}$) in perceptual discriminability. No statistically significant difference was noticed between vessel-restricted mapping and grayscale (t-test $p = 0.0527$, Wilcoxon $p = 0.0679$). In contrast, vessel-restricted mapping showed a significant improvement over full-image cosine mapping ($p < 10^{-6}$) in OPR. Vessel-restricted mapping exhibited lower inversion compared to full-image cosine mapping, with marginal statistical significance (t-test $p = 0.0422$, Wilcoxon $p = 0.0679$).

E. Qualitative Visualization

To complement the quantitative and statistical analyses, qualitative comparisons of grayscale, full-image cosine, and vessel-restricted cosine representations are shown in Fig. 11. Fig. 11 presents three views: axial slice visualization, maximum intensity projection (MIP), and a zoomed region highlighting local vascular structures.

V. Discussion

Fig. 2 indicates that vascular structures occupy a sparse and distinct region of the intensity space, while Fig. 3 indicates that the extracted mask lines up with anatomical vessels. Fig. 4 indicates that the vessel mask captures bright vascular structures while suppressing surrounding tissue responses. As shown in Table I, the vessel restricted cosine method preserves the original information. Whereas full-image cosine mapping introduces major structural distortions, as evidenced by lower SSIM scores and higher NMSE values. Global intensity ordering remains fairly strong, but inversion artifacts reveal how periodic color modulation disrupts local relationships. Vessel-restricted mapping, however, maintains nearly perfect structural fidelity and minimizes these inversion issues. By confining the transformation to vessels only, it avoids the distortions seen in the full-image approach. Vessel-restricted cosine mapping increases chromatic discriminability without alteration to luminance-based structure.

Table II and Figs. 5–10 show that the patterns revealed in the single case generalize across the multiple images. Vessel-restricted mapping closely matches the grayscale baseline in structural measures while providing improved chromatic separability, while full-image cosine mapping consistently shows degraded structural metrics and reduced perceptual clarity. The lower inversion in vessel-restricted representations, compared to full cosine mapping, further emphasizes the stability of the localized approach. In particular, Figs. 5-6 confirm structure preservation, Figs. 7-8 indicate stable intensity ordering with little inversion, and Figs. 9-10 demonstrate vessel-background perceptual distinction and local contrast behavior.

The statistical analysis shows that substantial improvements in perceptual discriminability ($\Delta E_{d'}$) were noted when comparing vessel-restricted mapping to both grayscale and full-image cosine representations. At the same time, the lack of

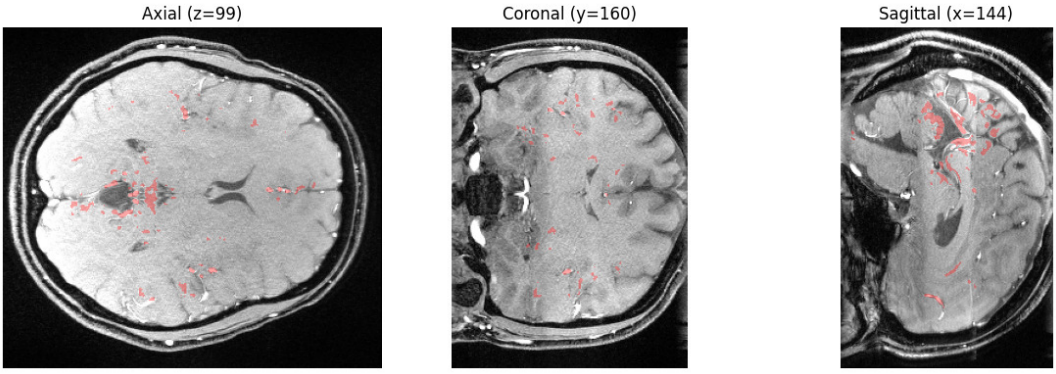

Fig. 4. Extracted vessels overlay.

TABLE I
QUANTITATIVE COMPARISON OF GRAYSCALE, FULL-VOLUME COSINE MAPPING, AND VESSEL-RESTRICTED COSINE MAPPING.

Method	**NMSE**	**SSIM**	**OPR**	**Inv.**	$L_{d'}$	**Chroma**$_{d'}$	ΔE_{mean}	$\Delta E_{d'}$	**Local C.**
Gray	0.000000	1.000000	0.998405	0.000000	0.749028	0.732236	10.146879	0.224801	0.083883
Full	0.018082	0.847326	0.997503	0.015662	0.750136	0.601273	8.909666	0.236465	0.072914
Vessel	0.000001	0.999993	0.998405	0.000000	0.748340	0.795021	10.190250	0.232772	0.083362

TABLE II
QUANTITATIVE COMPARISON ACROSS METHODS (MEAN $\pm$ STANDARD DEVIATION).

Method	**NMSE**	**SSIM**	**OPR**	**Inv.**	$L_{d'}$	**Chr**$_{d'}$	ΔE_m	$\Delta E_{d'}$	**Loc. C.**
Gray	0.0000 ± 0.000	1.0000 ± 0.000	0.9971 ± 0.002	0.0000 ± 0.000	0.7512 ± 0.061	0.7365 ± 0.0596	10.9066 ± 0.6462	0.1945 ± 0.0728	0.0901 ± 0.0085
Full	0.0176 ± 0.0017	0.8500 ± 0.0181	0.9956 ± 0.0024	0.0030 ± 0.0060	0.7515 ± 0.0609	0.6476 ± 0.0629	9.5393 ± 0.5529	0.2065 ± 0.0733	0.0781 ± 0.0073
Vessel	0.0000 ± 0.0000	1.0000 ± 0.0000	0.9971 ± 0.0016	0.0000 ± 0.0000	0.7504 ± 0.0604	0.8306 ± 0.0847	10.9527 ± 0.6471	0.2018 ± 0.0714	0.0896 ± 0.0085

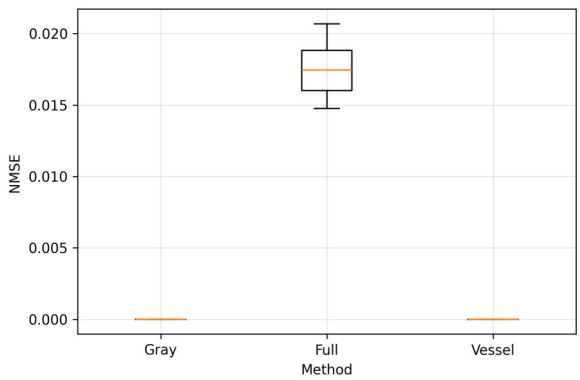

Fig. 5. Boxplot comparison of NMSE.

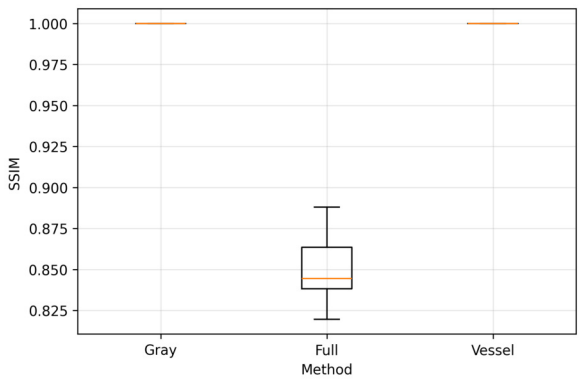

Fig. 6. Boxplot comparison of SSIM.

significant differences in object preservation between vessel-restricted mapping and grayscale suggests that the vessel cosine mapping maintains structural reliability while enhancing perceptual discriminability.

From Fig. 11, the grayscale appearance of surrounding tissue is preserved as in the case of vessel-restricted cosine mapping while confining chromatic variations to vessel regions. Whereas global color distortions and intensity inconsistencies are introduced with the use of full-image cosine mapping, which affects both vascular and non-vascular regions. The result from Fig. 11 shows that vessel-restricted cosine mapping provides localized perceptual enhancement while preserving anatomical fidelity.

This study is limited by the use of 20 healthy MRA volumes from a 61-volume corpus. The cosine parameters were fixed, standard sequential or diverging colormaps were not compared, and luminance analysis used Rec. 709 convention.

VI. CONCLUSION

The effectiveness of cosine mapping is highly dependent on its spatial application. Full-image cosine mapping introduced measurable structural distortion, with reduced structural sim-

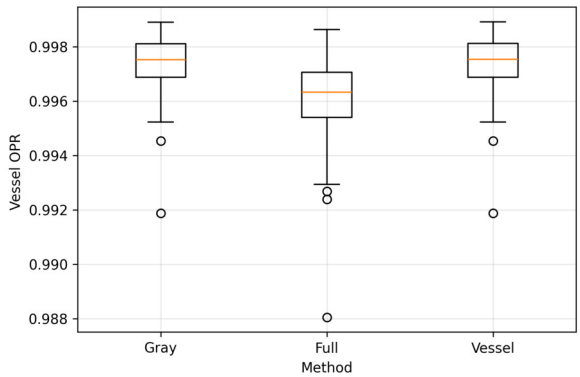

Fig. 7. Boxplot comparison of OPR.

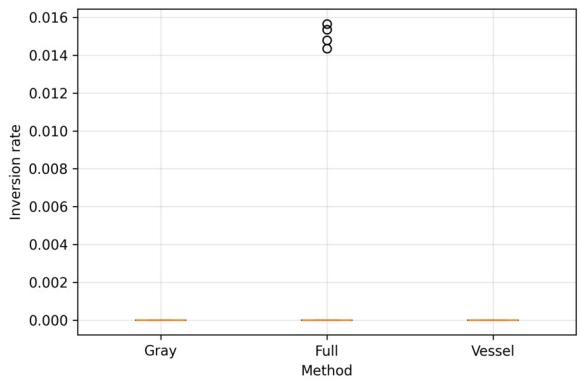

Fig. 8. Boxplot comparison of inversion rate.

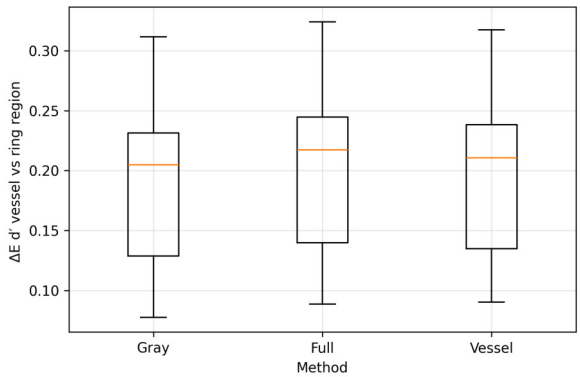

Fig. 9. Boxplot comparison of vessel ring metric.

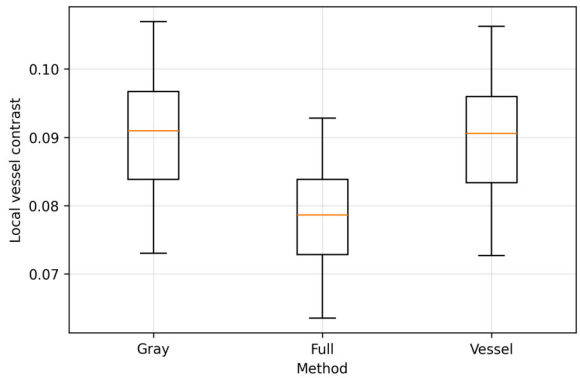

Fig. 10. Boxplot comparison of local vessel contrast.

ilarity ≈ 0.85 and increased reconstruction error of ≈ 0.018, along with non-zero inversion artifacts of ≈ 0.003. Although global intensity ordering remained relatively high with a value of $\approx 0.9950.8$, full-image mapping reduced chromatic discriminability of ≈ 0.65. In contrast, vessel-restricted cosine mapping preserved anatomical structure with a near-perfect fidelity with an error of ≈ 0 and a structural similarity value of ≈ 1.0, and eliminated inversion artifacts of 0.000, while maintaining object preservation comparable to grayscale of ≈ 0.997. Importantly, it improved chromatic discriminability ≈ 0.83 relative to both grayscale ≈ 0.74 and full-image cosine mapping and achieved slightly improved perceptual separation of $\Delta E_{\text{mean}} of \approx 10.95$. These improvements were statistically significant, $\Delta E_{d'}$ showing strong significance when comparing vessel-restricted mapping to grayscale and full-image cosine (paired t-test $p < 10^{-6}$, Wilcoxon $p < 10^{-5}$).

Qualitative analysis suggested that vessel-restricted mapping provides localized chromatic enhancement of vascular structures while preserving the grayscale appearance of surrounding tissue, avoiding the global distortions observed in full-image cosine mapping.

The proposed vessel-restricted approach therefore shows a favorable balance between enhancement and fidelity, suggesting its potential as a visualization-oriented enhancement

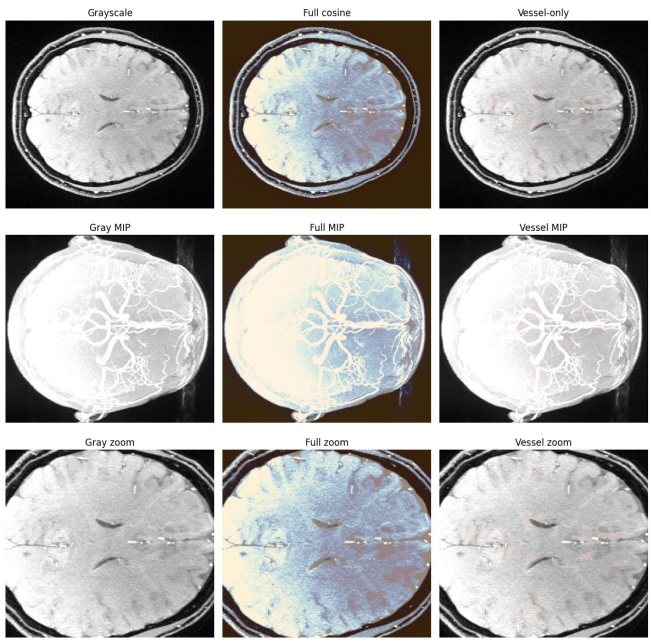

Fig. 11. Qualitative comparison of grayscale, full-image cosine, and vessel-restricted cosine representations across slice, MIP, and zoomed views.

method for MRA. A promising direction for future work is to explore optimization strategies to select cosine mapping parameters for maximizing perceptual discriminability while preserving structural constraints. Additionally, utilizing global perceptual metrics and task-based clinical evaluation will be important to assess the broader impact of the method on diagnostic performance.

DATA AND CODE AVAILABILITY

Data underlying the results presented in this paper are publicly available at https://www.nitrc.org/projects/icbmmra/. The source code used for preprocessing, cosine colorization, vessel-restricted masking, and metric evaluation is available upon reasonable request from the correcponding author.

ACKNOWLEDGMENT

The study is funded by the Lithuanian Research Council (LMT) under project grant number S-PD-25–40. During the preparation of this work, the authors used OpenAI tools to help refine and improve the code for the experiments. They also used Grammarly to review and improve the manuscripts' grammar. The authors take full responsibility for the content of this publication.

REFERENCES

[1] Gadhave DG, Sugandhi VV, Jha SK, Nangare SN, Gupta G, Singh SK, Dua K, Cho H, Hansbro PM, Paudel KR. Neurodegenerative disorders: Mechanisms of degeneration and therapeutic approaches with their clinical relevance. Ageing research reviews. 2024 Aug 1;99:102357, https://doi.org/10.1016/j.arr.2024.102357.

[2] Rezaei M, Mohammadikhaveh S, Faraji H, Ardalani R, Rezaei M, Shirazinodeh A. Early diagnosis of Alzheimer's disease based on brain morphological changes: A comprehensive approach combining voxel-based morphometry and deep learning. NeuroImage: Reports. 2026 Mar 1;6(1):100315, https://doi.org/10.1016/j.ynirp.2025.100315.

[3] BAlsabti SM, Al-Gburi RM, Mustafa A, AHMED SK, Issa AM, Al-Naimi TM, AlSaad R, Elhenidy AM. Advances in Deep Learning for Multimodal Brain Imaging: A Comprehensive Survey. Neuroscience Informatics. 2025 Dec 19:100252, https://doi.org/10.1016/j.neuri.2025.100252.

[4] Karthikeyan S, Muthu Kumar B, Kiran ML, Srivatsan K. Computational Brain Imaging Framework for Neurological Mapping and Disorder Classification Using Multimodal Image Processing. International Journal of Computational Intelligence Systems. 2025 May 19;18(1):121, https://doi.org/10.1007/s44196-025-00852-1.

[5] Ricci M, Cimini A, Chiaravalloti A, Filippi L, Schillaci O. Positron emission tomography (PET) and neuroimaging in the personalized approach to neurodegenerative causes of dementia. International Journal of Molecular Sciences. 2020 Oct 11;21(20):7481, https://doi.org/10.3390/ijms21207481.

[6] Ansari AS, Mohammadi MS, Cattani C, Tassaddiq A. An advanced multimodal image fusion model for accurate detection of Alzheimer's disease using MRI and PET. Frontiers in Medical Technology. 2025 Dec 2;7:1699821, https://doi.org/10.3389/fmedt.2025.1699821.

[7] Bhattacharya S, Prusty S, Pande SP, Gulhane M, Lavate SH, Rakesh N, Veerasamy S. Integration of multimodal imaging data with machine learning for improved diagnosis and prognosis in neuroimaging. Frontiers in Human Neuroscience. 2025 Mar 21;19:1552178, https://doi.org/10.3389/fnhum.2025.1552178.

[8] Zubair M, Hussain M, Al-Bashrawi MA, Bendechache M, Owais M. A comprehensive review of techniques, algorithms, advancements, challenges, and clinical applications of multi-modal medical image fusion for improved diagnosis. Computer Methods and Programs in Biomedicine. 2025 Sep 9:109014, https://doi.org/10.1016/j.cmpb.2025.109014.

[9] Calhoun VD, Sui J. Multimodal fusion of brain imaging data: a key to finding the missing link (s) in complex mental illness. Biological psychiatry: cognitive neuroscience and neuroimaging. 2016 May 1;1(3):230-44, https://doi.org/10.1016/j.bpsc.2015.12.005.

[10] Mathur AN, Khattar A, Sharma O. 2D to 3D medical image colorization. InProceedings of the IEEE/CVF Winter Conference on Applications of Computer Vision 2021 (pp. 2847-2856), https://doi.org/10.1109/WACV48630.2021.00289.

[11] Odusami M, Damasevicius R, Milieskaite-Belousoviene E, Maskeliunas R. Multimodal neuroimaging fusion for Alzheimer's disease: an image colorization approach with mobile vision transformer. International Journal of Imaging Systems and Technology. 2024 Sep;34(5):e23158, https://doi.org/10.1002/ima.23158.

[12] Pei E. Ambient Environment Effect on Color Perception. Rochester Institute of Technology; 2025.

[13] Costanzo L, Failla G, Aluigi L, Baroncelli TA, Bua C, De Marchi S, Diaco E, Di Paola F, Di Pino FL, Mannello F, Martinelli O. Operative Procedures for Ultrasound Assessment of Extracranial Artery Disease: A Narrative Review by the Italian Society for Vascular Investigation (SIDV). Journal of Clinical Medicine. 2025 Oct 6;14(19):7050, https://doi.org/10.3390/jcm14197050.

[14] Alfadeel H. Impact of CT Stroke Window Settings on Acute Stroke Detection. Scientific Journal of University of Benghazi. 2025 Jun 29;38(1):193-214, https://doi.org/10.37376/sjuob.v38i1.7328.

[15] D'Angelo T, Mastrodicasa D, Lanzafame LR, Yel I, Koch V, Gruenewald LD, Sharma SP, Ascenti V, Micari A, Blandino A, Vogl TJ. Optimization of window settings for coronary artery assessment using spectral CT-derived virtual monoenergetic imaging. La radiologia medica. 2024 Jul;129(7):999-100 7, https://doi.org/10.1007/s11547-024-01835-6.

[16] Mohammad NI. Hierarchical Spatial Algorithms for High-Resolution Image Quantization and Feature Extraction. arXiv preprint arXiv:2510.08449. 2025 Oct 9, https://doi.org/10.1049/iet-ipr.2019.0921.

[17] Singh N, Bhandari AK. Image contrast enhancement with brightness preservation using an optimal gamma and logarithmic approach. IET Image Process 14 (4): 794–805 [Internet]. 2019

[18] Sarkar K, Halder TK, Mandal A. Adaptive power-law and cdf-based geometric transformation for low-contrast image enhancement. Multimedia Tools and Applications. 2021 Feb;80(4):6329-5 3, https://doi.org/10.1007/s11042-020-10004-6

[19] Khan MA, AlGhamdi MA. An intelligent and fast system for detection of grape diseases in RGB, grayscale, YCbCr, HSV, and L*a*b* color spaces. Multimedia Tools and Applications. 2024 May;83(17):50381-99, https://doi.org/10.1007/s11042-023-17446-8

[20] Mookiah S, Parasuraman K, Kumar Chandar S. Color image segmentation based on improved sine cosine optimization algorithm. Soft Computing. 2022 Dec;26(23):13193-203, https://doi.org/10.1007/s00500-022-07133-5

[21] Reinhold JC, Dewey BE, Carass A, Prince JL. Evaluating the impact of intensity normalization on MR image synthesis. In Proceedings of SPIE—the International Society for Optical Engineering, 2019 Mar (Vol. 10949, p. 109493H), https://doi.org/10.1117/12.2513089.

[22] Johnson R. A review of three-dimensional medical image visualization. Health Data Science. 2022(1):83-101, https://doi.org/10.34133/2022/9840519.

[23] Longo A, Morscher S, Najafababdi JM, Jüstel D, Zakian C, Ntziachristos V. Assessment of a Hessian-based Frangi vesselness filter in optoacoustic imaging. Photoacoustics. 2020 Dec 1;20:100200, https://doi.org/10.1016/j.pacs.2020.100200

[24] Sheethal. M. S, Amudha P. Enhanced Brain Tumor Detection via Multiscale Frangi Gaussian Matrix and Efficient Convolutional Networks on MRI. J. Inf. Hiding Multim. Signal Process. 2024 Sep;15(4):236-70.

[25] Qin B, Jin M, Hao D, Lv Y, Liu Q, Zhu Y, Ding S, Zhao J, Fei B. Accurate vessel extraction via tensor completion of background layer in X-ray coronary angiograms. Pattern recognition. 2019 Mar 1;87:38-54, https://doi.org/10.1016/j.patcog.2018.09.015.

[26] Zhang M, Wang J, Cao X, Xu X, Zhou J, Chen H. An integrated global and local thresholding method for segmenting blood vessels in angiography. Heliyon. 2024 Nov 30;10(22), https://doi.org/10.1016/j.heliyon.2024.e38579.

[27] Recommendation IT. Colour conversion from Recommendation ITU-R BT. 709 to Recommendation ITU-R BT. 2020. Geneva: ITU-R. 2015.